Molecular Dynamics Study on the Crystallization of a Cluster of Polymer Chains Depending on the Initial Entanglement Structure

Xiang Yu, Bin Kong, and Xiaozhen Yang*

Beijing National Laboratory for Molecular Sciences, Joint Laboratory of Polymer Science and Materials, State Key Laboratory of Polymer Physics and Chemistry, Institute of Chemistry, Chinese Academy of Sciences, Beijing 100190, China

Received January 24, 2008; Revised Manuscript Received July 9, 2008

ABSTRACT: Using a large polymer chain cluster, we have examined entanglement densities of the polymer chains in the bulk and in the surface by molecular dynamics simulation. The entanglement density was measured by the interchain contact fraction (ICF), which was developed as a structural parameter of the entanglement. It was found that the surface location has a lower ICF than the bulk core does. Different entanglement structures then underwent crystallization processes. It resulted in a multidomain system, in which the directors of the order domains are in isotropic distributed. For calculating the crystallinity of the systems, we developed a method, the site order parameter (SOP), which endows local order to every particle in the system; when determining the order for crystalline phase, one can count the crystallinity. SOP enables us to transform a molecular chain picture into an order image, where white stands for the crystalline phase and black for the amorphous. Snapshots of the simulations show evolution of the nucleation and the crystal growth through SOP images. The dynamic effect of the entanglement was observed in the crystallization behaviors. It shows that the entanglement has a higher density in the bulk and a lower density in the surface. The result shows that a shorter induction period of nucleation and a higher crystal growth rate was found in the surface location, since possessing lower ICF.

1. Introduction

The study of polymer entanglement has been one of the most important aspects in polymer science, and a great number of research works have been done in this area. Like Doi−Edwards' tube model, most of them[1−5] were developed for the bulk polymer system, and they match some experiments. However, the polymer entanglement density was found to be changed under confinement such as at the surface or interface, which is different from the situation in bulk. Brown and co-workers[6,7] reported the decrease of entanglement density near the surface and the interface theoretically. Si and co-workers[8] discovered that when a thin glassy film was strained uniaxially, the thinner the film was, the higher maximum extension ratio it would reach, indicating that the entanglement density decreased with film thickness. Meyer et al.[9] simulated the dynamics and disentanglement in thin and two-dimensional polymer films. They analyzed the impact of confinement on the entanglement length N_e by the primitive path analysis and found that N_e increases strongly with decreasing film thickness, showing the decreased entanglement density in the thin films. Guerin et al.[10] proposed a geometrical model to describe the decrease of glass transition temperature with the decreasing film thickness and reported that this phenomenon is due to the modification of the interpenetration between neighboring chains, which results in expressed chain motion by the presence of surface in the free-standing thin films.

Study on behavior of polymer chain systems with different degrees of entanglement, in the bulk or in the confinement circumstance, is an interesting subject. Crystallization of the systems is considered to be one of the effective ways to examine the behavior of the entanglements. The influence of the entanglement on the crystallization has been proved by some experiments. Bu et al.[11,12] prepared single- and pauci-chain collective particles from dilute solutions of isotactic polystyrene in benzene and found that crystallization rate of the collective particles is much faster than that of bulk polymer. It is attributed to the much fewer entanglements in the collective particles, thus indicating that the entanglements could be a barrier to the crystallization of polymers. Psarski[13] prepared molten polyethylene from extended crystals, which was expected to have fewer entanglements, and found the crystallization rate of the melt is increased by 25−45% compared to that of the ordinary entangled melt. Hikosaka and Yamazaki et al.[14−16] prepared polymer melt with postulated entanglement densities (ν_e), and then crystallization was performed. It was observed that the nucleation rate decreases with the increase of the entanglement density exponentially.

Computer simulation has gradually come to front to show capability of describing changes in microstructure at the atomistic level, which is difficult to observe directly in experiments. Many computer simulation studies[17−25] have been carried out to simulate polymer crystallization, but few are related to the entanglement. The difficulties in quantifying the entanglement density and in producing structures with different global or local entanglement densities give rise to a situation that only a few simulation works have been done on this aspect. In our previous work,[26] the interpenetration degree model has been introduced. The interpenetration degree is expected to be one of the structural attributes of the entanglement in polymer system. This concept has been introduced in the early stage of crystallization of a six-chain polyethylene system.[27] In this pauci-chain system, effect of the entanglement on crystallization was clearly found. However, the six-chain system used in ref 27 was so small that it was similar to the situation in poor solution but not in the bulky polymer with surface. In order to study the entanglement near the surface, a much larger system is required. Thus, a system containing 45 000 atoms was used in the present work. It is expected that many crystalline domains will appear in the system after crystallization.

In order to measure the crystallization rate in such a large system, an effective method measuring crystallinity should be used. The frequently used methods to measure the crystallinity include the ordinary method to calculate global order parameter introduced by Muthukumar, Rutledge, and Meyer[17,19,22] and the

* To whom all correspondence should be addressed. E-mail: yangx@iccas.ac.cn.

10.1021/ma800172t CCC: $40.75
Published on Web 08/22/2008

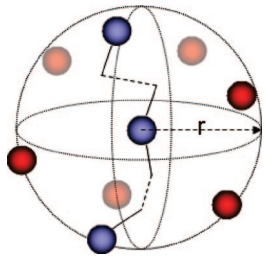

Figure 1. Interchain contact fraction model.

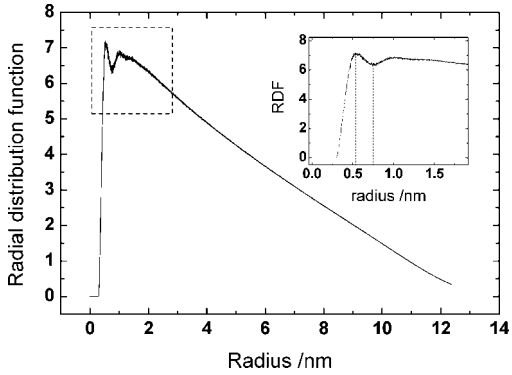

Figure 2. Radial distribution function of methylene in the amorphous coil.

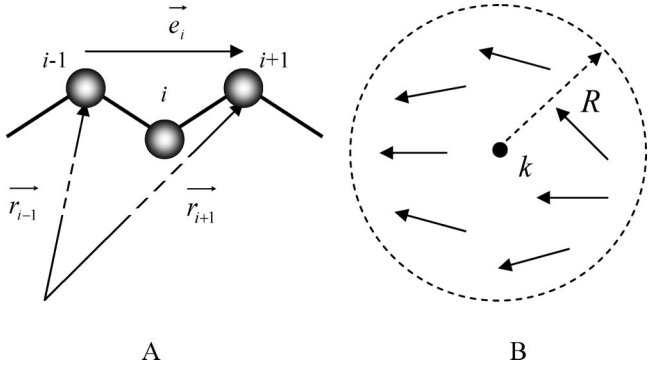

Figure 3. (A) Unit orientation vector of site *i*. (B) Site order parameter model.

modified method to calculate local order parameter layer by layer such as in Rutledge et al.'s work.[23] Since there exist different phases and several crystalline domains in the large system, in which the two highly ordered vectors in different crystalline domains would result in long-range counteractions, it thus needs development.

In the present work, crystallization behaviors of the large polymer chain systems with different entanglement densities, characterized by the structural parameter of entanglement introduced by us before,[26] have been studied. A new method has been developed from previous works to measure order parameter of a multidomain system. This method proved to be effective in describing the crystalline nuclear size, the crystallinity, the local nucleation rate, and the crystal growth rate. Obtained results provide the local entanglement difference between the surface and the bulk of polymer chain system.

2. Model and Methodology

2.1. Simulation Details. The polymer molecules considered in this paper are polyethylenes, and they consist of united-atom CH_2. There are two systems with different sizes. One has 16 300-CH_2 chains, and it is named as *the small system*. The other has 150 300-CH_2 chains, and it is named as *the large system*. After crystallization, a single crystalline domain formed in the small system while several domains formed in the large system.

Molecular dynamics simulation is performed by the open source software package GROMACS 3.3.1.[28,29] The parameters used for simulation were derived from Dreiding II force field.[30] As the temperature used in this simulation work was higher than real experiment in order to obtain an equilibrium amorphous state as soon as possible, the normalized temperature was used. We set the normalized temperature $T_n = 1.0$, which stands for the real temperature of 1000 K, for simulation of interpenetration, and the simulation of crystallization was performed from $T_n = 0.3-0.6$. A Nose-Hoover type thermostat algorithm with a relaxation time of 0.1 ps was used. The integration time step was set to be 0.002 ps.

The small system was simulated as follows: 16 globules each of which consists of 300 CH_2 united atoms were put in a cubic box (by using the tool "genconf" in the software package), and then the box was removed and the system was put in vacuum circumstances; meanwhile, the 16 globules were kept in correlated positions. After that, interpenetration process was simulated for 12 ns at $T_n = 1.0$. Thus, an amorphous coil was produced. Then crystallization was simulated with the sample quenching from $T_n = 0.8-0.3$ at a decline rate of 0.025 T/ns, then the temperature was set to be $T_n = 0.3$, and the crystallization was simulated for another 4 ns. After this process, a final structure with a single crystallized domain was obtained.

The way of simulating the large system was similar to the small system. The interpenetration of 150 300-CH_2 globules was first simulated at $T_n = 1.0$ for 30 ns, and then six initial structures were extracted from the trajectory file at different times. All the six structures would be used as the initial structures of crystallization. The simulation of crystallization was performed at the temperature $T_n = 0.6$ for 12 ns.

2.2. Interchain Contact Fraction. To quantify the interpenetration of the chains, we introduced a parameter named interchain contact fraction (ICF). ICF is correlated to the degree of interpenetration and entanglement of the system. Briefly, for a given monomer, a fraction of monomers as the first neighbor belonging to another chain can be found (Figure 1). In the present work, ICF was used to characterize the entanglement density. It is calculated as follows:

$$G_{\text{inter}}(r) = \frac{N_{\text{inter}}(r)}{N_t 4\pi r^2\, \mathrm{d}r} \tag{1}$$

$$G_{\text{total}}(r) = \frac{N_{\text{total}}(r)}{N_t 4\pi r^2\, \mathrm{d}r} \tag{2}$$

$$\text{ICF} = \frac{\sum G_{\text{inter}}(r_1)}{\sum G_{\text{total}}(r_1)} = \frac{\sum N_{\text{inter}}(r_1)}{\sum N_{\text{total}}(r_1)} \tag{3}$$

Here $N_{\text{inter}}(r)$ is the number of interchain atoms around certain atom at distance r, and $N_{\text{total}}(r)$ is the number of total atoms ($N_{\text{total}}(r) = N_{\text{inter}}(r) + N_{\text{intra}}(r)$) around the same atom. N_t is the total number of atoms in the entire space of simulation system. The total volume is normalized. Thus, $G_{\text{inter}}(r)$ is the radial distribution function of interchain atoms, and $G_{\text{total}}(r)$ is the radial distribution function of total atoms. The ICF could be derived from $\sum G_{\text{inter}}(r_1)/\sum G_{\text{total}}(r_1)$ when the distance is equal to r_1, at which the first neighbor peak appears. From Figure 2, it could be concluded that this peak appears at the distance of 0.5 nm, and actually the r ranging from 0.48 to 0.52 nm was used. In the present work, the ICF was calculated by $\sum N_{\text{inter}}(r_1)/\sum N_{\text{total}}(r_1)$, both numerator and denominator were counted by the computer.

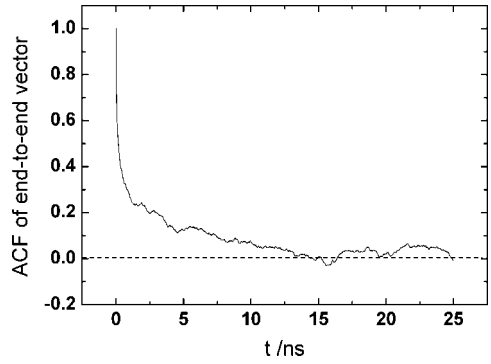

Figure 4. Autocorrelation function of end-to-end vector for the interpenetration process at high temperature.

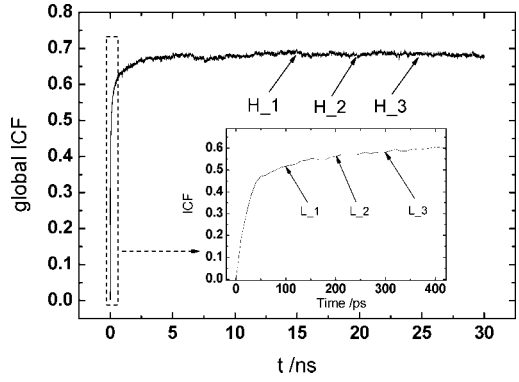

Figure 5. ICF of the large system during interpenetration process and the moments to extract the six structures.

Table 1. ICF of Six Structures Extracted from Interpenetration Process

	L-group			H-group		
structure	L_1	L_2	L_3	H_1	H_2	H_3
time/ps	100	200	300	15000	20000	25000
global ICF	0.517	0.561	0.581	0.693	0.678	0.689

2.3. Site Order Parameter. The site order parameter (SOP) was proposed in the present study. This method is based on a consideration that a given site in the system can be endowed with an order parameter which results from the order described by several vectors around in certain angstroms of radius. SOP really measures the order parameter of every site in polymer chain system.

In a polymer chain, for an atom i which does not locate at the end of the chain, there is an orientation vector which points from atom $i-1$ to atom $i+1$, and it could be normalized to a unit vector, just as Figure 3A shows.

$$\vec{e}_i = (\overrightarrow{r_{i+1}} - \overrightarrow{r_{i-1}})/|\overrightarrow{r_{i+1}} - \overrightarrow{r_{i-1}}| \tag{4}$$

For two given orientation vectors $\vec{e}_i$ and $\vec{e}_j$ (φ is the cross angle), the order parameter between them is calculated as follows:

$$P_{ij} = \frac{3\cos^2\varphi - 1}{2} = \frac{3}{2}(\vec{e}_i \cdot \vec{e}_j)^2 - \frac{1}{2} \tag{5}$$

The ordinary method to calculate the order parameter is to find all possible P_{ij} in the system, just as Muthukumar[17] and Rutledge[22] did. Meyer[19] alternated this method to find two bond vectors at certain distance in the whole system. These calculations were designed for average global order parameters. Rutledge et al.[23] proposed a method to calculate the local order parameter for each selected layer perpendicular to the depth of thin films.

Now a modification was made in the SOP method to meet the needs of measuring local order of every site or particle even in multidomain systems. Figure 3B shows the definition of SOP. Around the site k, there are a number of orientation vectors in the first neighbor shell domain, and SOP is obtained by calculating the average order parameter of any pair of orientation vectors in the domain. To avoid the influence of nearby bonds, the vectors on the same chain within three bonds from the site were excluded. The radius of the domain R was set to be 0.7 nm because the first peak on the radial distribution function (RDF) curve (Figure 2) decreases to a local minimum value at a distance of 0.7 nm. The order parameter of kth site is calculated as follows, where i and j stand for any two orientation vectors in the domain:

$$\mathrm{SOP}_k = \frac{\langle 3\cos^2(\varphi) - 1\rangle}{2} = \frac{3}{2}\langle(\vec{e}_i \cdot \vec{e}_j)^2\rangle_R - \frac{1}{2} \tag{6}$$

For the entire system that contains N sites, the order parameter of the system is calculated by averaging SOP of all sites in the system:

$$\bar{P} = \frac{1}{N}\sum_{k=1}^{N} \mathrm{SOP}_k \tag{7}$$

Also, it is convenient to calculate the crystallinity of a polymer system by the ratio

$$f_c = \frac{N_{cv}}{N} \tag{8}$$

where N_{cv} is the number of sites with SOP higher than a critical value ($\sim$0.7) and N is the number of total sites.

Furthermore, we have alternated the radius R of local domain from 0.3 to 1.5 nm. No significant difference of SOP was found in crystalline domain. But we found that if R decreases from 0.7 to 0.3 nm, the SOP obtained for amorphous phase would increase from 0.05 to 0.20 or even higher value, indicating the existence of oriented structure nearby in small domain. Then if R increases from 0.7 to 1.5 nm, the SOP obtained for amorphous phase would decrease from 0.05 to 0.01 or even lower. Thus, if R is larger than 1.0 nm, the SOP measurement of amorphous phase would be more precise. However, we think that there is no significant difference for the SOP value of amorphous phase between 0.05 and 0.01; meanwhile, the critical value $R = 0.7$ nm has a physical meaning. And actually, the CPU time of measuring SOP would increase exponentially with R^6. For these reasons, we set R at the critical value of 0.7 nm.

With this R value, the number of orientation vectors in the spherical domain was counted for a different phase: in the completely amorphous phase, the number was about 40−50; in the highly ordered phase, this number can reach up to 70; at the place very close to the surface this number will decrease to less than 30. The reason is that above the surface a few tails of polymer chains are free-standing and isolated in vacuum. Since some vectors along the tail are likely to be parallel to each other, SOP calculated from such a low-density domain with deficient samples was found to result in a wrong description of the structure. In order to avoid the misinterpretation that measured order from the tail is as high as that from the crystalline structure, SOP of such sites is therefore set to be zero.

3. Results and Discussion

3.1. Different Entanglement Structures around Surface and Bulk Domain. As mentioned in section 2.1, the large system underwent an interpenetration process. In order to produce initial structures with different entanglement densities, six snapshots were extracted from trajectory of the interpenetration process.

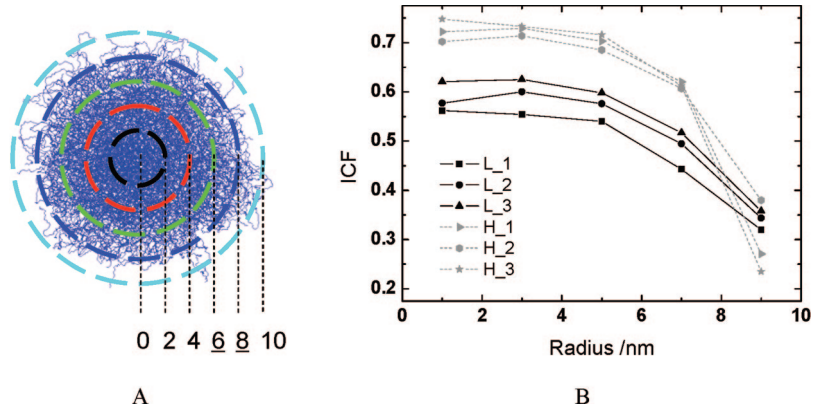

Figure 6. (A) A core and four shells for the amorphous coil. (B) ICF of each shell of the six structures.

Figure 4 shows the autocorrelation function of end-to-end vector for this interpenetration process. The curve shows that the system is getting into equilibrium state. Figure 5 shows the global ICF evolution of the system and the moment these six snapshots were picked up. The six initial structures are in two groups: the L-group and H-group. The three structures in L-group were picked up at very early stages (less than 500 ps), and the global ICF is 0.52, 0.56, and 0.58 for L_1, L_2, and L_3; the three structures in H-group were picked up at quite late stage (beyond 10 ns) with the global ICF of 0.69, 0.68, and 0.69 for H_1, H_2, and H_3. The details are listed in Table 1.

From Figure 4, it is indicated that the interpenetration process reaches the equilibrium state after about 12.5 ns. Thus, the structures of H-group are fully equilibrated, but those of L-group are not. It is experimentally realizable to start crystallization from the nonequilibrated structures. Nowadays, the single chain globules can be easily prepared and heated to make the chains interpenetrated with different degrees[12] can be achieved. The samples with various ICF values can be obtained by quenching the interpenetrated globules at different stages.

More detailed information about the entanglement density distribution of the six initial structures was exposed by analysis of ICF distribution along the radius. For the analysis, the system was divided into a core and four shells. The thickness of each shell is 2.0 nm, just as Figure 6A shows. We calculated the mass density distribution along the radius for the system and found the diameter of the sphere to be ~16 nm. It is indicated that the shell 6−8 nm is the surface shell, and the shell 8−10 nm is the one with little structure above the surface. Then the structural features of the entanglement described by ICF calculated for each shell and the core are shown in Figure 6B. The figure clearly shows that ICF has a plateau from the core and the density starts to decrease at the shell 6−8 nm (the surface shell). This indicates that the surface has lower ICF than the central part does. In other words, the surface has topological structure, which tends to form a weak entanglement.

The system thus provides two different entanglement structures: the surface shell and the bulklike core. The former has low ICF, and the latter has a high value. Such characteristic matches the result of Brown and co-workers.[6,8] They performed an experiment on a shear deformed zone for a stretched thin glassy film; the results prove that polymers in thin films are less entangled than bulk polymers. Because of the high ratio of surface part in the film, only when the entanglement at the surface is weaker than that in bulk can this result be obtained. Therefore, we have discussed the rationality of the ICF description in terms of structural attributes of the entanglement. However, the entanglement also has dynamic attributes; we have to examine various ICF structures in a chain motion process.

Table 2. Moments and Global Order Parameter of Each Snapshot in the Small System

snapshot number	s1	s2	s3	s4	s5	s6	s7
time/ps	260	5980	7080	7780	8420	10920	24000
SOP (global)	0.10	0.20	0.30	0.40	0.50	0.60	0.69

In the following sections the polymer chain crystallization will be mentioned in examination of the dynamic attributes of the entanglement.

3.2. Crystallization Examination in Various Entanglement Systems. *3.2.1. Definition of Crystallinity.* The nucleation rate is very important for computer simulation of crystallization. First and foremost, we have to measure the crystallinity of the system before obtaining the rate. For this purpose, the small system with single crystalline domain was simulated as mentioned in the section 2.1. Since the crystallinity is a fraction of the crystalline phase in the system, it is based on the two-phase model: the crystalline phase and the noncrystalline phase. It is important to find out a critical order, above which is in the crystalline phase. Using this value, we can divide the system into two phases and have the crystallinity.

For obtaining the critical value, seven snapshots which describe the crystallization process were extracted from the trajectory file (Table 2), and they were analyzed by using SOP. Their global SOP, which are calculated by eq 7, are approximately equal to 0.1, 0.2, 0.3, 0.4, 0.5, 0.6, and 0.7 for s1, s2, s3, s4, s5, s6, and s7, respectively.

Dealing with the single domain system, we are able to find the formation of nucleus through SOP, which is shown in Figure 7. Data in this figure were measured in a tube, which is along a line which passes through the mass center of the system and is parallel to the direction of the main crystalline domain from s2 to s7. The s2 structure shows SOP profile lower and fluctuating, but s3 shows a peak with SOP obviously higher

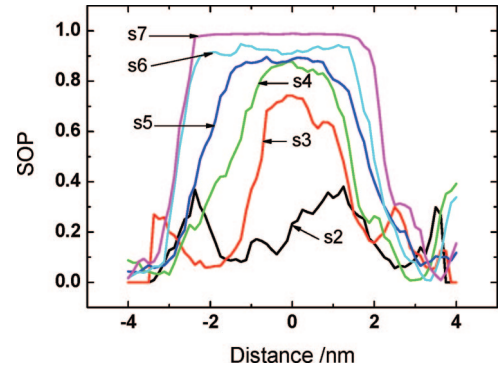

Figure 7. SOP along a line which passes through the mass center and is parallel to the main crystalline orientation in structures s2 to s7.

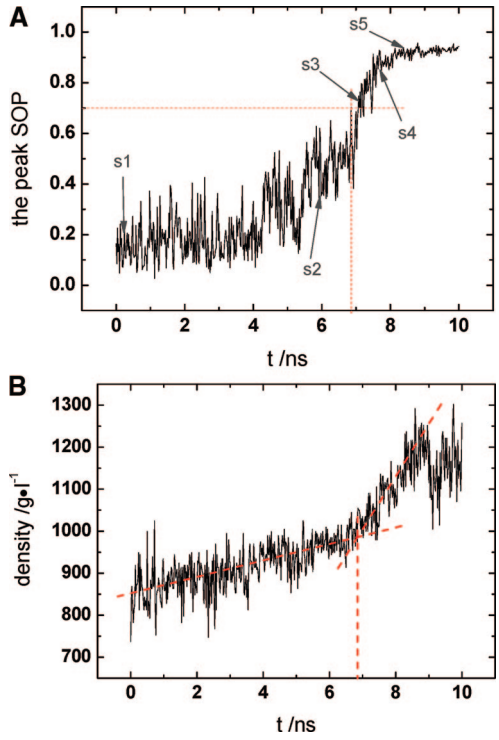

Figure 8. (A) Peak SOP along a line which is 3 nm in length and passes through the mass center and is parallel to the main crystalline orientation during the crystallization. (B) Mass density of a central column which is parallel to the main crystalline orientation and with 3 nm in length and 0.7 nm in radius.

than 0.7. From s4 to s7, the plateau of the curves become higher and wider.

Obviously, the SOP along the central highest value of the peaks shows a crystallization process in the single domain system. Such SOP as a function of time was traced for the first 10 ns as shown in Figure 8A. The snapshots of s1 to s5 are labeled in the figure, and snapshots of s6 and s7 are beyond the axis scale. Since the crystallization starts from amorphous structure, there must be a nucleation process. It is expected that in the process SOP range will cover the critical order value, before which huge fluctuation happens and after which the peak height simply increases and the peak width simply extends. It was found that at ~6.9 ns the SOP peak reaches ~0.7. Obviously, below this value SOP of the system fluctuates to a large extent, and above this value the fluctuation turns out to be relatively smaller. It is considered to be a turning point at this moment. This phenomenon indicates that an effective nucleus is being formed before ~6.9 ns. Data in Figure 8B support the conclusion. The slope of mass density of a column along the same line as Figure 8A (a tube of 0.7 nm in radius and 3 nm in length) versus time curve has a turning point around ~6.9 ns. Before the point the mass density increase was accompanied by a stable nucleus formation. After this turning point the crystal growth starts immediately. Results reveal that the turning points of SOP peaks and the mass density are coincident, at which the SOP is close to 0.7. We thus think 0.7 is the right critical SOP value to differentiate the crystalline structure from noncrystalline structure.

As the critical SOP of nucleation was found, it is reasonable to consider that the local domain where SOP is as high as 0.7 should be regarded as a baby nucleus and one can calculate the crystallinity by counting the percentage of atomic sites with SOP above 0.7 (eq 8).

By using the definition of crystallinity, we analyzed the large systems, which are multidomain systems. Before the SOP

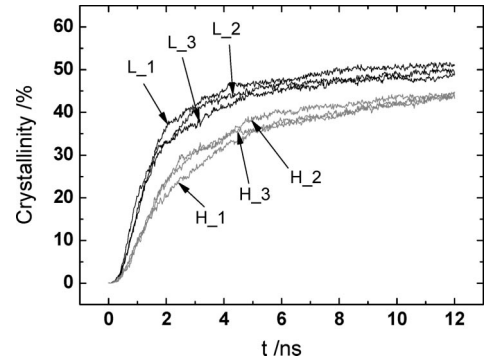

Figure 9. Crystallinity evolutions of six systems: the black curves for the L-group and the gray curves for the H-group.

method was introduced in the large system, the general orientation function was usually used and vectors of ordered domains in different directors were found to be counteracted with each other which results in a distortion of the orientation degree. SOP is a localized order and is good for multidomain system. We used the SOP crystallinity and traced the global crystallinity evolution of the six samples with different ICF values, as shown in Figure 9. This figure shows that the L-group has an obviously higher crystallization rate compared with the H-group, which matches the conclusion from experiments,[11−16] since ICF correlates closely with the entanglement density. This result supplements our early study[27] that in the multidomain system the same phenomenon (higher rate with low ICF) occurs as well as in the single domain system.

3.2.2. SOP Images of Nucleation in Multidomain System. Using SOP, we are able to transform the order parameter to images of the chain system at any moment to describe the evolution of crystallization even in multidomain system. By this method, we monitored the evolution of two large sphere systems with different global ICF: 0.52 for L_1 and 0.68 for H_2 as mentioned in the section 3.1. Figure 10 shows SOP imaging for these two samples. It should be noted that these images were not taken for the entire system, but each of them stands for the central sliced layer with a thickness of 2 nm of each system. Both the surface and the bulklike core are exposed in these images.

In the images, the black points denote the sites having SOP close to zero, and the white points have SOP near unity. The gray points have ordered structures in between. Now we have evolution of structural order parameter showed by SOP images. At the beginning, both structures L_1 and H_2 appear almost in black because they are completely amorphous. At 200 ps, both samples are embedded with many small light domains, whose sizes are less than 2 nm. The small domains are located almost evenly. At 500 ps, most of the domains grow up a bit. The bigger domains in H_2 are located around the surface shell, and in both samples some light domains appear with their sizes about 2 nm. At 1 ns, H_2 shows three stable ordered domains after the small domains merged or disappeared. L_1 shows more than six ordered domains which are more obvious than before. The results manifest that both systems underwent nucleation process, and crystallization can take place everywhere in the L_1 system while it could not occur in the interior region in the H_2 system. The following images prove the different nuclear growth processes. On the other hand, one can find a new nucleation occurred, which results in four ordered domains in H_2. In view of the domain direction or stem direction, one can distinguish domains from one another. During the same period, the small domains in L_1 merged and finally L_1 has nearly two big domains.

Through the analysis before, three conclusions can be drawn: (i) The appearance or disappearance of the small light spots

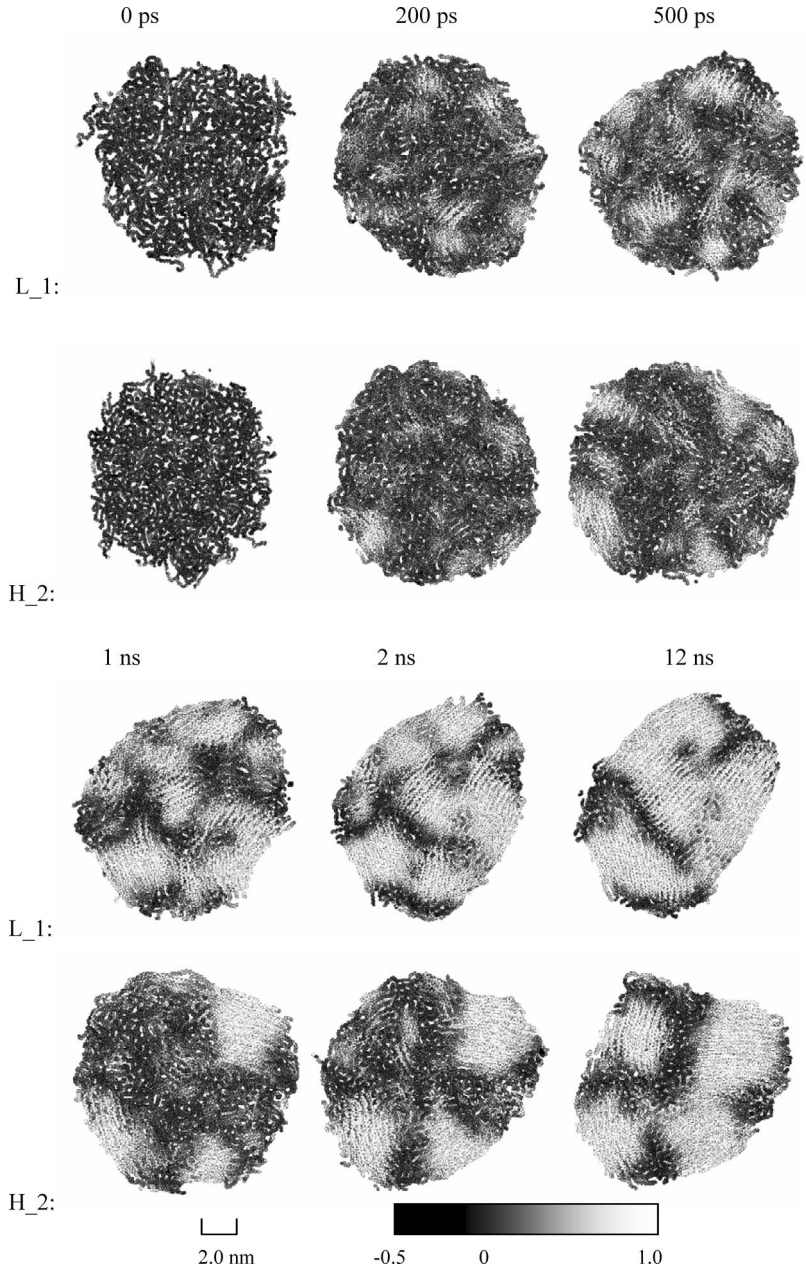

Figure 10. Six snapshots of 0 ps, 200 ps, 500 ps, 1 ns, 2 ns, and 12 ns with information on SOP images for L_1 and H_2 systems. The black point stands for the site with low SOP and the light gray point the opposite.

describes the nucleation fluctuation. (ii) The degree of crystallinity can be estimated by the lightness of the white region in the images, and it is observed that the low ICF image, L_1, always has a higher degree of crystallinity than the high ICF image, H_2, does at every moment. (iii) The nucleation occurs only around the surface region for the high ICF system, but it occurs from both the surface region and the central core for the low ICF system.

3.2.3. Crystallization Process. SOP images gave a direct and clear view for the local nucleation and crystallization growth. It is obvious that reasonable estimation of the evolution of the two processes can be made by using the images. For further study, quantified description for these systems is also needed. It is already known that nucleation process only occurs at surface of the H_2 system while it occurs everywhere in the L_1 system. For convenience, each of the six systems was divided into two regions: the interior region and the exterior region. The interior region is chosen as the central spherical space whose radius is 3 nm, and the exterior region includes all the other sites that beyond this spherical space. Then the crystallinity evolutions for each region were measured by eq 8.

Figure 11 shows the crystallinity of the interior and the exterior part varies with time in the first 2 ns of crystallization in both L_1 and H_2 systems. In this figure, an induction period of the crystallization or a nucleation stage can be approximately found from 0 to ~500 ps. In this period, the curve maintains near zero, and SOP of all particles fluctuates under 0.7 in the systems. Then crystallinity of each curve becomes slightly larger, and then the crystallinity goes up linearly as time goes on. The last stage is obviously the crystal growth stage. It also reveals that before the last stage there exists a period when crystallinity is beyond zero and under the value for crystal growth stage to take place. This is because a number of nuclei are forming; meanwhile, crystal growth from a few existed nuclei is undergoing.

In order to examine the influence of various initial structures on the crystallization behavior, the induction period or the nucleation duration is a suitable indicator. Figure 11 shows that

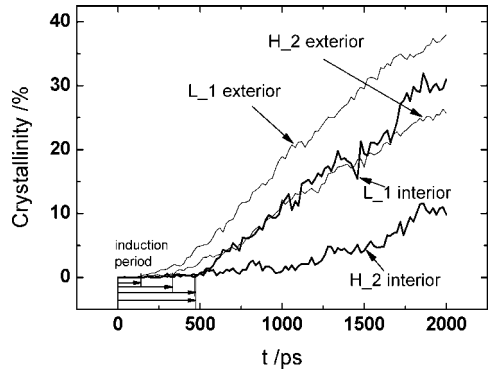

Figure 11. Crystallinity of interior and exterior part of L_1 and H_2 systems varies with time.

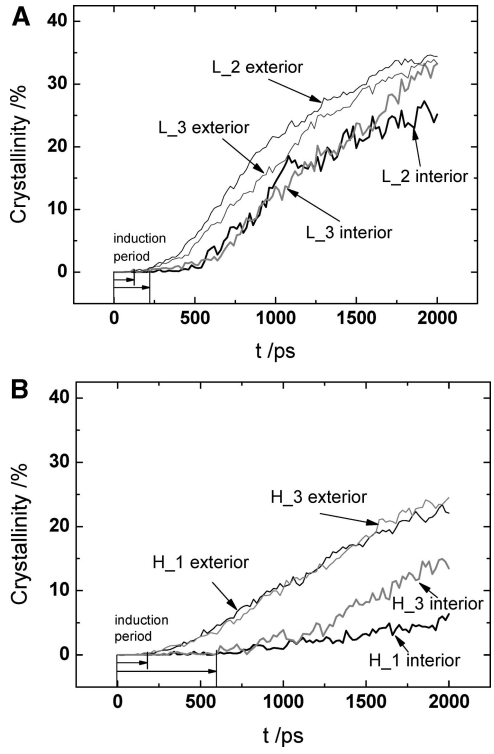

Figure 12. Crystallinity of interior and exterior part of all other systems (excluded with L_1 and H_2) varies with time.

(i) the induction period is ∼130 ps for L_1 exterior, ∼330 ps for H_2 exterior, ∼470 ps for L_1 interior, and ∼480 ps for H_2 interior, thus either interior or exterior part in L_1 has a shorter induction period than the same part in H_2 does; (ii) either interior or exterior parts in L_1 has a higher crystal growth rate than the same part in H_2 does; (iii) the exterior part of both L_1 and H_2 has a shorter induction period and a higher crystal growth rate than the interiors do; (iv) the exterior part of H_2 has the same crystal growth rate as the interior part of L_1 does, although the former has a shorter induction period than the latter one does.

Evolution of crystallinity in interior part and exterior part for other systems was also traced. Figure 12 shows evolutions for L_2, L_3, H_1, and H_3 systems. In Figure 12A, it was found that the exterior part in both L_2 and L_3 systems have the slightly shorter induction period than their interior parts do. In Figure 12B, for the H_1 and H_3 systems, the order of the induction period for the two parts is the same as that in L_2 and L_3 systems, but the crystallinity difference between the exterior part and the interior part becomes much larger.

These phenomena can be considered to have correlation with the entanglements. The shorter induction period and higher crystal growth rate in L-group indicates that the L-group has lower entanglement density than the H-group does. Compared with the interior part of both L-group and H-group, the exterior part has both shorter induction period and higher crystal growth rate, which indicates the lower entanglement density at the surface than at the bulk core. In section 3.1, entanglement density has been alternatively measured by using ICF. Figure 6B indicates that structures in L-group have lower ICF than those in H-group do; meanwhile, the surface part in both L- and H-groups have lower ICF than the central core does.

Moreover, the surface part of the H-group has nearly the same ICF as the central part of the L-group does. Therefore, it is concluded that the structures with similar entanglement density (measured by ICF) are expected to have similar crystallization behaviors. Through the analysis of Figure 11 and Figure 12, one found that three L-group interior samples have almost the same slopes of crystal growth lines and so do three H-group exterior samples. In other words, the crystal growth curves of the six samples from the two groups nearly overlap with each other, which is just like the curves for L_1 and H_2 in Figure 11. The result manifests that the interior L-group and the exterior H-group have nearly the same ICF, and the two local domains may have roughly the same crystallization rates. But their nucleation behaviors, or the induction period, were found to be different. It proves that the exterior region does have the shorter induction period than the interior one does.

4. Conclusion

The entanglement distribution for the amorphous polymer sphere was studied by using ICF analysis. Six samples were extracted from the trajectory of interpenetration and were divided into two groups: the H-group with high global ICF values and the L-group with low values. A plateau at the central core and a descent at the surface were found on the curves of ICF versus radius for each sample. As ICF is an approach to measure the entanglement density for amorphous polymer, it can be concluded that the entanglement density at the surface is lower than the bulk core; therefore, two different entanglement domains are provided: the bulk and the surface.

A modified method SOP in measuring order parameter of a system from every local site order parameters was proposed in the present work. In this method, each site was endowed with an order parameter which was calculated from all orientation vector pairs within certain radius. The most obvious advantage of using this method to quantify the order degree of a complex polymer system with many crystalline and amorphous domains is its capability to avoid long-distance counteraction of two orientation vectors in different crystalline domains. The SOP method can provide an order parameter more precisely than ordinary methods do for more complicated multidomain systems. A critical SOP of nucleation was found to be ∼0.7, and the crystallinity was defined as percentage of the sites where SOP is higher than this value. With this definition, the crystallization process was traced by evolution of the crystallinity with time.

The evolution of six systems with different initial structures was traced by calculating the crystallinity, and it was found that the samples with higher global ICF values have higher crystallization rate while the samples with lower values have lower crystallization rate, indicating the obvious depress effect of entanglement on crystallization in multidomain systems, which supplements our early study in the pauci-chain system.

Then the SOP images of central sliced layers were taken for two samples: one has lower global ICF value and the other has higher value. From these images, both appearance and disap-

pearance of nuclei could be found, indicating the fluctuation of nucleation. Further analysis of these images reveals that in the sample with lower global ICF, the crystallinity was higher and the nucleation of the lower global ICF sample can occur everywhere in the system. On the other hand, in the sample with higher global ICF, the crystallinity was lower and the nucleation occurred only around the surface region.

At last, all the samples in both L-group and H-group were divided into two parts: the interior part within a spherical space whose radius is 3.0 nm and the exterior part that include all other domains beyond the interior part. The evolution of crystallinity for each part was traced. The shorter induction period and higher crystal growth rate found in L-group indicates the entanglement density of these structures is lower than that of those in the H-group, and the shorter induction period combined with higher crystal growth rate at the exterior part for both L- and H-groups indicates the entanglement density at the surface is lower than that in the bulk core. Moreover, the interior parts of three L-group samples have almost the same crystallinity evolution curves, and so do the exterior parts of three H-group samples. The reason can be attributed to the close entanglement density between the interior parts of L-group samples and the exterior parts of H-group samples.

Acknowledgment. We acknowledge the support from National Science Foundation of China (90612015, 20474073, 20490220, 20674090) and 973 (2004CB720606) projects.

References and Notes

(1) Lin, Y. H. *Macromolecules* **1987**, *20*, 3080–3083.
(2) Kavassalis, T. A.; Noolandi, J. *Macromolecules* **1988**, *21*, 2869–2879.
(3) Heymans, N. *Macromolecules* **2000**, *33*, 4226–4234.
(4) Wool, R. P. *Macromolecules* **1993**, *26*, 1564–1569.
(5) Wu, S. *J. Polym. Sci., Part B: Polym. Phys.* **1989**, *27*, 723–741.
(6) Brown, H. R.; Russell, T. P. *Macromolecules* **1996**, *29*, 798–800.
(7) Oslanec, R.; Brown, H. R. *Macromolecules* **2003**, *36*, 5839–5844.
(8) Si, L.; Massa, M. V.; Dalnoki-Veress, K.; Brown, H. R.; Jones, R. A. L. *Phys. Rev. Lett.* **2005**, *94* (12), 127801.
(9) Meyer, H.; Kreer, T.; Cavallo, A.; Wittmer, J. P.; Baschnagel, J. *Eur. Phys. J.: Spec. Top.* **2007**, *141*, 167–172.
(10) Guerin, G.; PruD'Homme, R. E. *J. Polym. Sci., Part B: Polym. Phys.* **2007**, *45*, 10–17.
(11) Bu, H. S.; Gu, F. M.; Bao, L. R.; Chen, M. *Macromolecules* **1998**, *31*, 7108–7110.
(12) Bu, H. S.; Gu, F. M.; Chen, M.; Bao, L. R.; Cao, J. *J. Macromol. Sci., Phys.* **2000**, *B39*, 93–108.
(13) Psarski, M.; Piorkowska, E.; Galeski, A. *Macromolecules* **2000**, *33*, 916–932.
(14) Yamazaki, S.; Hikosaka, M.; Toda, A.; Wataoka, I.; Gu, F. M. *Polymer* **2002**, *43*, 6585–6593.
(15) Hikosaka, M.; Watanabe, K.; Okada, K.; Yamazaki, S. *Adv. Polym. Sci.* **2005**, *191*, 137–186.
(16) Yamazaki, S.; Gu, F. M.; Watanabe, K.; Okada, K.; Toda, A.; Hikosaka, M. *Polymer* **2006**, *47*, 6422–6428.
(17) Liu, C.; Muthukumar, M. *J. Chem. Phys.* **1998**, *109*, 2536–2542.
(18) Muthukumar, M. *Adv. Polym. Sci.* **2005**, *191*, 241–274.
(19) Meyer, H.; Muller-Plathe, F. *Macromolecules* **2002**, *35*, 1241–1252.
(20) Xu, L.; Fan, Z. Y.; Zhang, H. D.; Bu, H. S. *J. Chem. Phys.* **2002**, *117*, 6331–6335.
(21) Yamamoto, T. *Adv. Polym. Sci.* **2005**, *191*, 37–85.
(22) Lavine, M. S.; Waheed, N.; Rutledge, G. C. *Polymer* **2003**, *44*, 1771–1779.
(23) Waheed, N.; Ko, M. J.; Rutledge, G. C. *Polymer* **2005**, *46*, 8689–8702.
(24) Gee, R. H.; Lacevic, N.; Fried, L. E. *Nat. Mater.* **2006**, *5*, 39–43.
(25) Lacevic, N.; Fried, L. E.; Gee, R. H. *J. Chem. Phys.* **2008**, *128*, 014903.
(26) Liang, T. N.; Zhang, Z. Q.; Li, T.; Yang, X. Z. *Polymer* **2004**, *45*, 1365–1371.
(27) Zhang, Z. Q.; Yang, X. Z. *Polymer* **2006**, *47*, 5213–5219.
(28) Van der Spoel, D.; Lindahl, E.; Hess, B.; Groenhof, G.; Mark, A. E.; Berendsen, H. J. C. *J. Comput. Chem.* **2005**, *26*, 1701–1718.
(29) Lindahl, E.; Hess, B.; van der Spoel, D. *J. Mol. Model.* **2001**, *7*, 306–317.
(30) Mayo, S. L., III *J. Phys. Chem.* **1990**, *94*, 8897–8909.

MA800172T